Observation of the room-temperature local ferromagnetism and its nanoscale expansion in the ferromagnetic semiconductor $Ge_{1-x}Fe_x$

Yuki K. Wakabayashi[1] and Yukio Takahashi[2]

[1] Department of Electrical Engineering and Information Systems, Tanaka-Ohya lab.

[2] Department of Physics, Fujimori lab. ([2] currently: Department of Physics, Komori lab.)

1. Authors

Yuki K. Wakabayashi : His major is semiconductor spintronics. He is investigating physical properties and device applications of the magnetic thin films which have high compatibility with the Si technology.

Yukio takahashi : His major is nanoscale magnetics. He is investigating magnetic materials by using X-ray magnetic circular dichroism (XMCD) and scanning Tunneing Microscope.

2. Introduction

A major issue that must be addressed for the realization of semiconductor spintronic devices is to achieve room-temperature ferromagnetism in ferromagnetic semiconductors (FMSs) based on the widely used III-V and group-IV materials. Recently, however, the group-IV-based FMS, $Ge_{1-x}Fe_x$ (GeFe) [1-6], has been reported to exhibit several attractive features. It can be grown epitaxially on Si and Ge substrates without the formation of intermetallic precipitates (Fig. 1), and is therefore compatible with mature Si process technology. The Curie temperature (T_C) can be easily increased to above 200 K by thermal annealing [4]. Furthermore, T_C does not depend on the carrier concentration, and thus T_C and resistivity can be controlled separately [3], which is a unique feature that is only observed in GeFe and is a considerable advantage in overcoming the conductivity mismatch problem between ferromagnetic metals and semiconductors in spin-injection devices. Despite these attractive features, a detailed microscopic understanding of the ferromagnetism in GeFe, which is vitally important for room-temperature applications, is lacking.

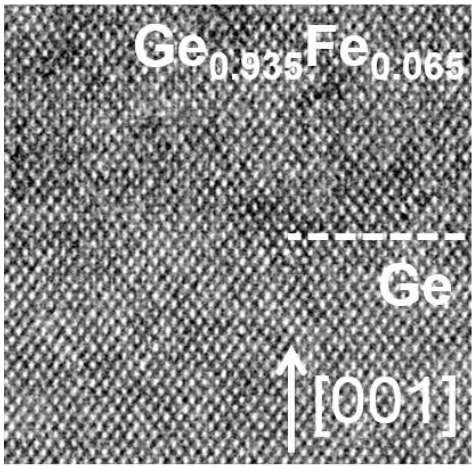

Figure 1. Transmission electron microscopy (TEM) lattice image of the $Ge_{0.935}Fe_{0.065}$ film.

3. Purpose of the study

Here, we investigate the local electronic and magnetic properties of GeFe using X-ray absorption spectroscopy (XAS) and X-ray magnetic circular dichroism (XMCD), which are powerful techniques for element-specific detection of local electronic states and magnetic moments [6]. We find that nanoscale local ferromagnetic regions remain in the GeFe films even at room temperature, i.e., well above T_C; it follows that GeFe potentially has strong ferromagnetism, which persists even at room temperature. Furthermore, we observe the intriguing feature that ferromagnetic regions, which are formed above T_C via the ferromagnetic exchange interaction in high-Fe concentration regions of the films, develop and expand as the temperature decreases, and that all of them coalesce at temperatures below T_C. Such a nanoscale

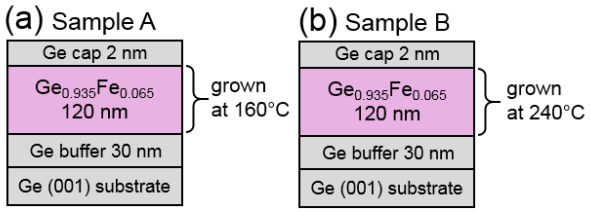

Figure 2. (a), (b) Schematic sample structures for sample A (a) and sample (b).

expansion of the ferromagnetic regions is a key feature in understanding materials that exhibit single-phase ferromagnetism despite the inhomogeneous distribution of magnetic atoms in the film.

4. Basic properties of our GeFe films

We carried out XMCD measurements on two samples (labeled A and B) consisting of a 120-nm-thick $Ge_{0.935}Fe_{0.065}$ layer grown on a Ge(001) substrate by low-temperature molecular beam epitaxy (LT-MBE). The $Ge_{0.935}Fe_{0.065}$ layer of sample A was grown at 160°C, whereas that of sample B was grown at 240°C (Fig. 2). We found T_C = 20 K and 100 K for samples A and B, respectively. Detailed crystallographic analyses, including *in situ* reflection high-energy electron diffraction (RHEED), high-resolution transmission electron microscopy (TEM), spatially resolved transmission-electron diffraction (TED) combined with energy-dispersive X-ray spectroscopy (EDX) and X-ray diffraction (XRD), showed that the GeFe films have a diamond-type single-crystal structure without any ferromagnetic precipitates and with nanoscale spatial Fe concentration fluctuations of 4% – 7% (sample A) and 3% – 10% (sample B) (Fig. 3). We found that T_C is higher when the fluctuations in the Fe concentration are larger. In addition, channeling Rutherford backscattering (c-RBS) and channeling particle-induced X-ray emission (c-PIXE) measurements showed that ~85% (~15%) of the doped Fe atoms exist at the substitutional (tetrahedral interstitial) sites in both samples A and B, and that the interstitial Fe

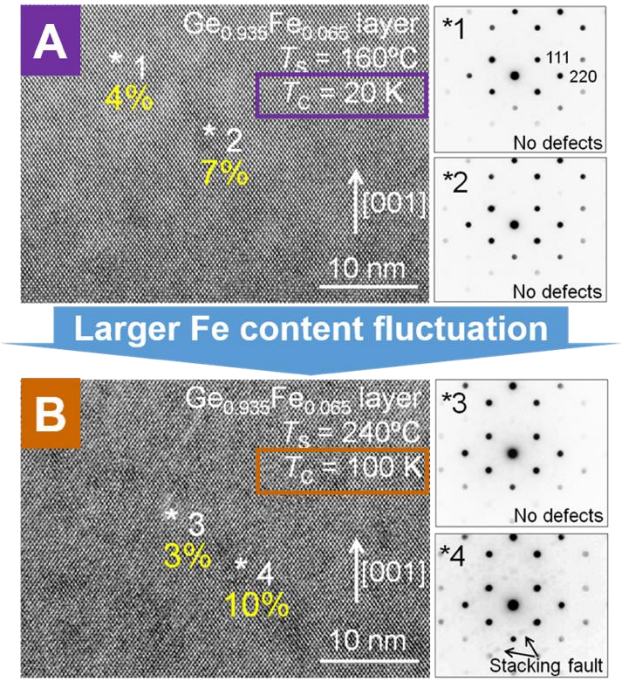

Figure 3. The TEM lattice images (left figures) and the TED patterns (right figures) for samples A and B.

concentration is not related to T_C. This also indicates that there are *no* ferromagnetic precipitates with different crystal structures in our films.

5. Results

We measured the Fe $L_{2,3}$-edge XAS spectra [μ^+, μ^- and $(\mu^+ + \mu^-)/2$] of samples A [Fig. 4(a)] and B [Fig. 4(b)] at 5.6 K with $\mu_0 H$ = 5 T applied perpendicular to the film surface. Here, μ^+ and μ^- refer to the absorption coefficients for photon helicity parallel and antiparallel to the Fe 3*d* majority spin direction, respectively. In both films, three peaks *a*, *b* and *c* are observed at the Fe L_3 edge in the XAS spectra [see also the insets in Fig. 4(a),(b)]. We found that the small peak *c* was suppressed by etching the surface with dilute HF, indicating that this peak, which can be assigned to the Fe^{3+} state, originates from a small quantity of surface Fe oxide, which remains even after surface cleaning. Meanwhile, peaks *a* and *b* are assigned to the Fe atoms in GeFe. Peaks *a* and *b* can be assigned to the Fe^{2+} state.

We measured the Fe $L_{2,3}$-edge XMCD (= $\mu^+ - \mu^-$)

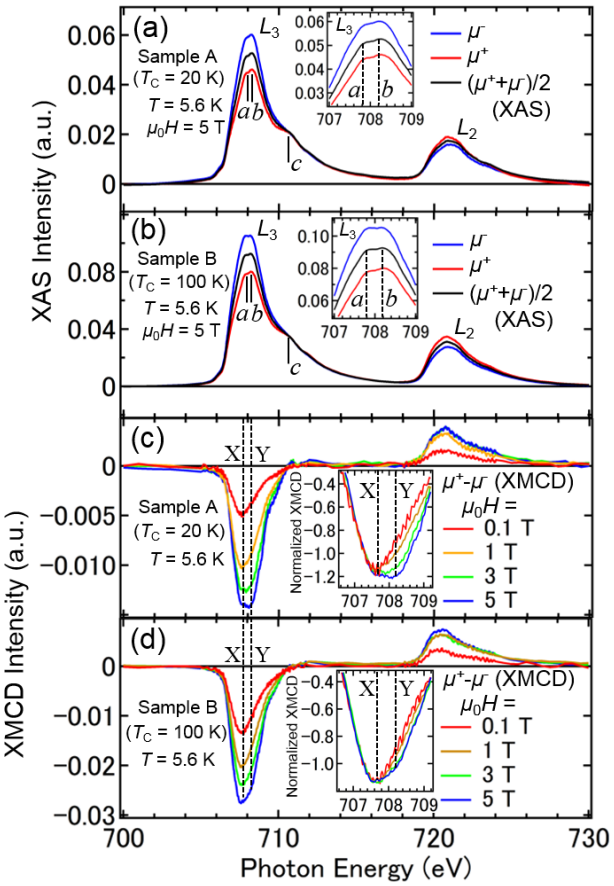

Figure 4. (a), (b) The dependence of the XMCD intensity measured at X on the effective magnetic field H_{eff} for sample A (a) and sample B (b) at various temperatures. The total magnetization ($M = m_{\mathrm{spin}} + m_{\mathrm{orb}}$) obtained using the XMCD sum rules is also plotted (filled red symbols). We scaled the vertical axis of the XMCD intensity so that it represents M at each temperature. In all measurements, H was applied perpendicular to the film surface.

spectra of samples A [Fig. 4(c)] and B [Fig. 4(d)] at 5.6 K with various H applied perpendicular to the film surface. Here, we discuss the XMCD intensities at 707.66 eV (X) and 708.2 eV (Y), which correspond to the photon energies of peaks *a* and *b* in the XAS spectra, respectively. When normalized to 707.3 eV, the XMCD spectra with various H differ, and the intensity at X grows faster than that at Y as H increases, as shown in the insets of Fig. 4(c),(d). As shown in Fig. 4(a),(b), the shapes of the XAS spectra at the Fe L_3 edge are similar between samples A and B, which have almost the same interstitial Fe concentrations (i.e., 15% of the total Fe content[6]); therefore, we can assign the XMCD intensity

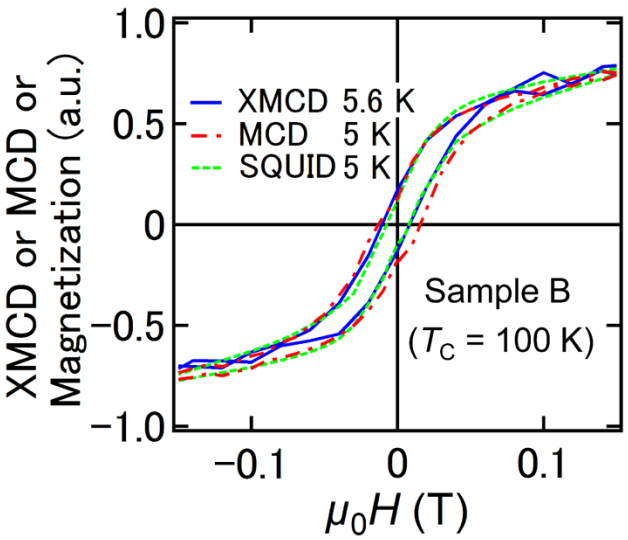

Figure 5. The H dependence of the XMCD intensity at X shown in Fig. 1 (707.66 eV) at 5.6 K, the MCD intensity at 5 K with a photon energy of 2.3 eV corresponding to the L-point energy gap of bulk Ge, and the magnetization measured using a SQUID at 5 K for sample B.

at X to the substitutional Fe atoms and the paramagnetic component of the XMCD intensity at Y to the interstitial Fe atoms. We do not observe fine structures due to multiplet splitting at the Fe L_3 edge in both samples, which would be observed if the 3*d* electrons were localized and were not strongly hybridized with other orbitals. These observations indicate that the Fe 3*d* electrons are strongly hybridized with the Ge 4*p* states.

Figure 5 shows the H dependence of the XMCD intensity at energy X and a temperature of 5.6 K, the MCD intensity measured with visible light of 2.3 eV at 5 K, and the magnetization measured using a SQUID at 5 K for sample B. The shapes of these curves show excellent agreement with each other; it follows that the spin splitting of the valence band composed of the Ge 4*p* orbitals is induced by the Fe 3*d* magnetic moment, which originates from the substitutional Fe atoms, through the *p*-*d* hybridization.

Figure 6(a),(b) shows the effective magnetic-field (H_{eff}) dependence of the XMCD intensity measured at X for samples A (a) and B (b) at various temperatures. Here, M is also plotted (filled red symbols), and $\mu_0 H_{\mathrm{eff}}$

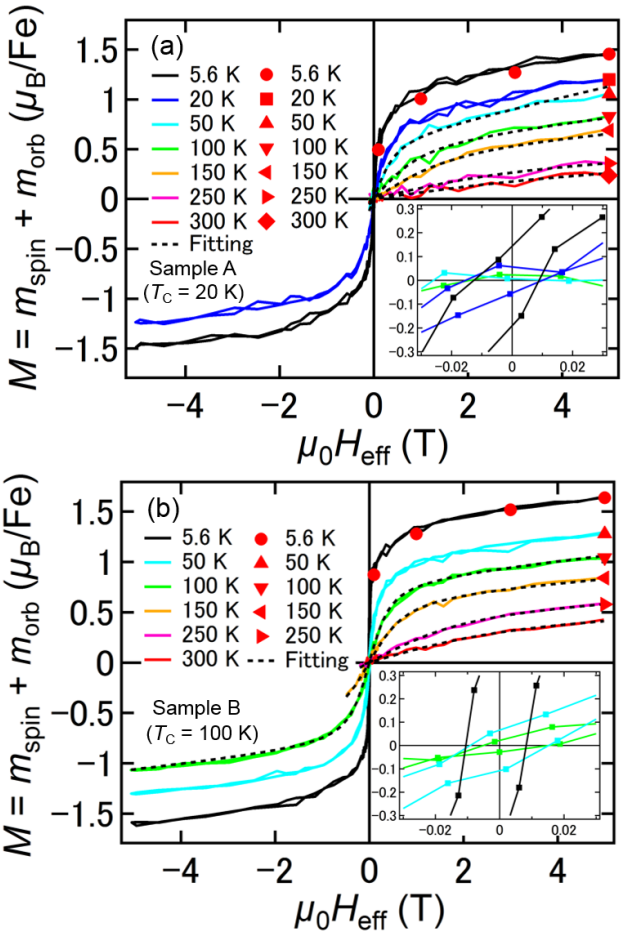

Figure 6. (a), (b) the effective magnetic-field (H_{eff}) dependence of the XMCD intensity measured at X for samples A (a) and B (b) at various temperatures.

is obtained by subtracting the product of M and the density of the substitutional Fe atoms from $\mu_0 H$ to eliminate the influence of the demagnetization field. The insets show clear hysteresis below T_C in both samples. The XMCD – H_{eff} curves show large curvature above T_C in both samples [see the main panels of Fig. 6(a),(b)], indicating that part of the film is superparamagnetic (SPM) above T_C. It indicates that local ferromagnetic regions form in nanoscale high-Fe concentration regions at temperatures above T_C, and thus M can be described by

$$M = 4.4\mu_B f_{SPM} L\left(\frac{m_{SPM}\mu_0 H_{eff}}{k_B T}\right) + (1\text{-}f_{SPM})\frac{C}{T}\mu_0 H_{eff}, \quad (1)$$

where f_{SPM} and m_{SPM} are fitting parameters expressing the fraction of SPM substitutional Fe atoms and the magnetic moment per local ferromagnetic region,

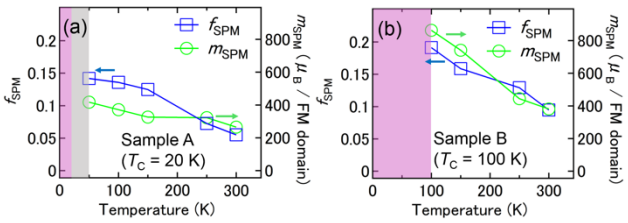

Figure 7. (a), (b) The temperature dependence of the best-fit parameters f_{SPM} and m_{SPM} obtained for sample A (a) and sample B (b). The red, grey, and white areas indicate ferromagnetic (FM), FM + SPM + paramagnetic (PM), and SPM + PM regions, respectively.

respectively. Also, C is the Curie constant per substitutional Fe atom, and L is the Langevin function. Here, 4.4μ_B is the *ideal* saturated value of M; i.e., $M = m_{spin} + (m_{orb}/m_{spin}) \times m_{spin}$, where $m_{spin} = 4\ \mu_B$ (for Fe^{2+}) and $m_{orb}/m_{spin} \approx 0.1$ when all the substitutional Fe atoms are magnetically active. Here, the Curie constant per substitutional Fe atom is obtained using the following equations:

$$C = \frac{\mu_B^2}{3k_B} n_B^2, \quad (2)$$

$$n_B = \left[\frac{3}{2} + \frac{S(S+1) - L(L+1)}{2J(J+1)}\right]\sqrt{J(J+1)}, \quad (3)$$

where μ_B, k_B, n_B, S, L and J represent the Bohr magneton, the Boltzmann constant, the effective Bohr magneton number, the spin angular momentum, the orbital angular momentum and the total angular momentum, respectively. Here, $S = 2$ (for Fe^{2+}), and $L = 0.4$ ($L = 2S \times m_{orb}/m_{spin}$, where $m_{orb}/m_{spin} \approx 0.1$), and $J = 2.4$ ($= L + S$ because the spin and orbital angular momenta of a substitutional Fe atom are parallel) in equation (3). Thus, n_B is estimated to be 5.24. The first and second terms in equation (1) correspond to the SPM and paramagnetic components, respectively. In Fig. 6(a),(b), the thin black solid curves correspond to the best fit obtained with equation (1). For sample B, the M – H_{eff} curves at temperatures in the range 100 – 300 K are well reproduced by equation (1), which indicates that the ferromagnetic – SPM transition occurs at T_C = 100 K. With sample A, the M – H_{eff} curves at

temperatures above T_C (i.e., $T \geq 20$ K) are well reproduced by equation (1), except for $T = 20$ K, which is probably due to the onset of ferromagnetism. These good fits up to room temperature indicate that ferromagnetic interactions within the nanoscale high-Fe concentration regions remain at room temperature in both samples.

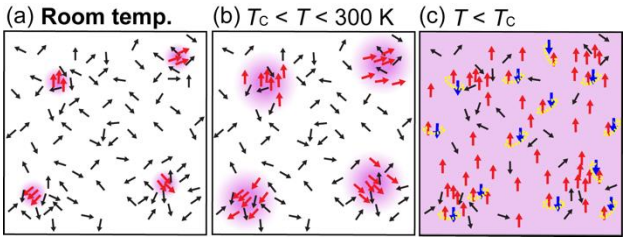

Figure 8. (a) – (c) Schematic diagrams showing the most likely picture of the magnetic states in the $Ge_{0.935}Fe_{0.065}$ films with zero magnetic field at room temperature (i.e., $T = 300$ K) (a), $T_C < T < 300$ K (b) and $T < T_C$ (c). The small black and red arrows correspond to the magnetic moments of the paramagnetic and ferromagnetic substitutional Fe atoms, respectively. The red areas indicate ferromagnetic regions.

We see a similar trend in the temperature dependence of the fitting parameters f_{SPM} and m_{SPM} in both films; i.e., f_{SPM} and m_{SPM} both increase with decreasing temperature (Figs. 7(a) and 7(b)). This result implies that the ferromagnetic regions, which form only in the nanoscale high-Fe concentration regions at room temperature [Fig. 8(a)], expand toward lower Fe concentration regions with decreasing temperature [Fig. 8(b)], and finally the entire film becomes ferromagnetic at T_C [Fig. 8(c)]. This appears to be a characteristic feature of materials that exhibit single-phase ferromagnetism, despite the inhomogeneous distribution of magnetic atoms in the film. As shown in Fig. 7(a),(b), f_{SPM} and m_{SPM} are larger in sample B than in sample A, which can be attributed to the difference in spatial fluctuations of the Fe concentration, which are 4% – 7% in sample A and 3% – 10% in sample B. The larger the nonuniformity of the Fe distribution is, the larger each local ferromagnetic region, $f_{SPM,}$ and m_{SPM} become, and the local ferromagnetic regions can be more easily connected magnetically, resulting in a higher T_C.

6. Summary

We have investigated the local electronic structure and magnetic properties of the doped Fe atoms in the $Ge_{0.935}Fe_{0.065}$ films, which have a diamond-type single-crystal structure without any ferromagnetic precipitates and with nanoscale spatial Fe concentration fluctuations, using XAS and XMCD. The fitting results clearly show that the local ferromagnetic regions, which exist at room temperature, expand with decreasing temperature, leading to a ferromagnetic transition of the entire system at T_C. The nonuniformity of the Fe concentration seems to play a crucial role for the formation of the ferromagnetic regions, and our results indicate that strong ferromagnetism is inherent to GeFe, and persists at room temperature. Such a nanoscale expansion of the ferromagnetic regions is a key feature in understanding materials that exhibit single-phase ferromagnetism (i.e., where the film is free from any ferromagnetic precipitates) despite the *inhomogeneous* distribution of magnetic atoms in the film.

7. Acknowledgements

We would like to special thanks our supervisors, Assoc. prof. S. Ohya, prof. A. Fujimori, Assoc. prof. K. Ishizaka and prof H. Takagi for their great supports and advises. We would thank MERIT program for providing the valuable collaborative research.

8. Publication and Award related to this study

[Award]

若林勇希、第 62 回(2015 年春季) 応用物理学会学術講演会 第三回英語講演奨励賞

[Publication]

Y. K. Wakabayashi, S. Sakamoto, Y. Takeda, K.

Ishigami, Y. Takahashi, Y. Saitoh, H. Yamagami, A. Fujimori, M. Tanaka, and S. Ohya, “Room-temperature local ferromagnetism and nanoscale domain growth in the ferromagnetic semiconductor GeFe”, Scientific Reports, **6** 23295 (2016).

References

[1] Y. Shuto, M. Tanaka, and S. Sugahara, phys. stat. sol. **3**, 4110 (2006).

[2] Y. K. Wakabayashi, S. Ohya, Y. Ban, and M. Tanaka, J. Appl. Phys. **116**, 173906 (2014).

[3] Y. Ban, Y. Wakabayashi, R. Akiyama, R. Nakane, and M. Tanaka, AIP Advances **4**, 097108 (2014).

[4] Y. K. Wakabayashi, Y. Ban, S. Ohya and M. Tanaka, Phys. Rev. B **90**, 205209 (2014).

[5] Y. K. Wakabayashi, S. Ohya, Y. Ban, and M. Tanaka, Appl. Phys. Express **9**, 123001 (2016).

[6] Y. K. Wakabayashi, S. Sakamoto, Y. Takeda, K. Ishigami, Y. Takahashi, Y. Saitoh, H. Yamagami, A. Fujimori, M. Tanaka, and S. Ohya, Scientific Reports, **9** 23295 (2016).